frontiers | Frontiers in Immunology

TYPE Original Research
PUBLISHED 17 December 2024
DOI 10.3389/fimmu.2024.1512470

OPEN ACCESS

EDITED BY
Heiko Mühl,
Goethe University Frankfurt, Germany

REVIEWED BY
Rebekka Lambrecht,
Weizmann Institute of Science, Israel
Bryan Copple,
Michigan State University, United States

*CORRESPONDENCE
Pedro Elias Marques
pedro.marques@kuleuven.be

RECEIVED 16 October 2024
ACCEPTED 29 November 2024
PUBLISHED 17 December 2024

CITATION
Vandendriessche S, Mattos MS, Bialek EL, Schuermans S, Proost P and Marques PE (2024) Complement activation drives the phagocytosis of necrotic cell debris and resolution of liver injury. *Front. Immunol.* 15:1512470. doi: 10.3389/fimmu.2024.1512470

Complement activation drives the phagocytosis of necrotic cell debris and resolution of liver injury

Sofie Vandendriessche, Matheus Silvério Mattos, Emilia Laura Bialek, Sara Schuermans, Paul Proost and Pedro Elias Marques*

Laboratory of Molecular Immunology, Department of Microbiology, Immunology and Transplantation, Rega Institute for Medical Research, KU Leuven, Leuven, Belgium

Cells die by necrosis due to excessive chemical or thermal stress, leading to plasma membrane rupture, release of intracellular components and severe inflammation. The clearance of necrotic cell debris is crucial for tissue recovery and injury resolution, however, the underlying mechanisms are still poorly understood, especially *in vivo*. This study examined the role of complement proteins in promoting clearance of necrotic cell debris by leukocytes and their influence on liver regeneration. We found that independently of the type of necrotic liver injury, either acetaminophen (APAP) overdose or thermal injury, complement proteins C1q and (i)C3b were deposited specifically on necrotic lesions via the activation of the classical pathway. Importantly, C3 deficiency led to a significant accumulation of necrotic debris and impairment of liver recovery in mice, which was attributed to decreased phagocytosis of debris by recruited neutrophils *in vivo*. Monocytes and macrophages also took part in debris clearance, although the necessity of C3 and CD11b was dependent on the specific type of necrotic liver injury. Using human neutrophils, we showed that absence of C3 or C1q caused a reduction in the volume of necrotic debris that is phagocytosed, indicating that complement promotes effective debris uptake in mice and humans. Moreover, internalization of opsonized debris induced the expression of pro-resolving genes in a C3-dependent manner, supporting the notion that debris clearance favors the resolution of inflammation. In summary, complement activation at injury sites is a pivotal event for necrotic debris clearance by phagocytes and determinant for efficient recovery from tissue injury.

KEYWORDS

necrosis, complement, phagocytosis, leukocytes, resolution

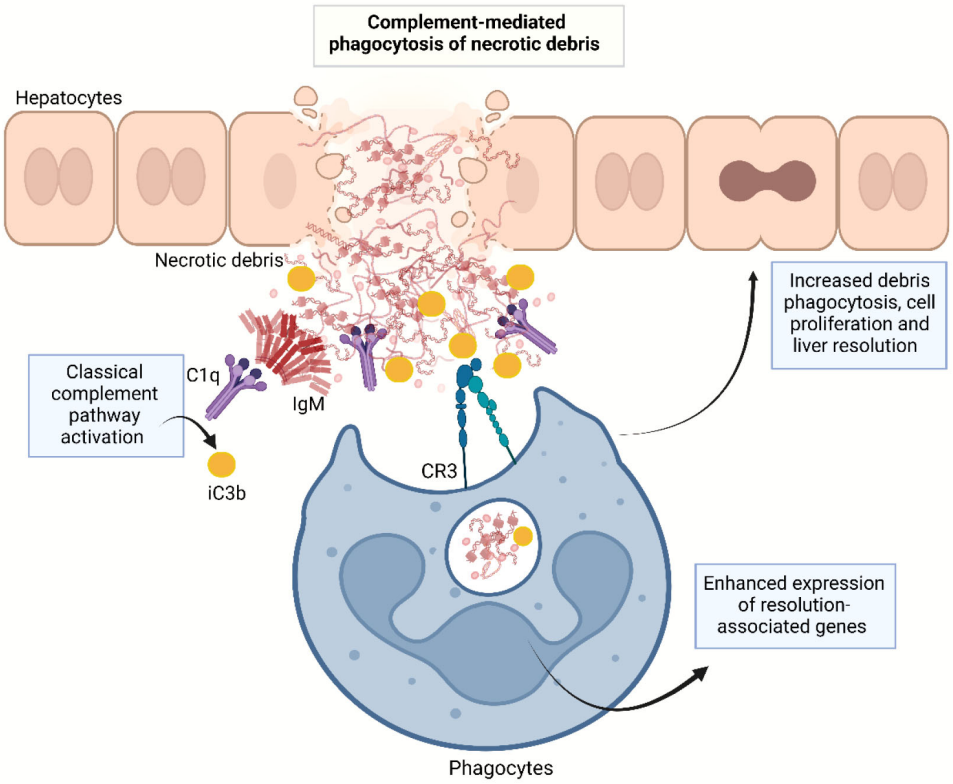

GRAPHICAL ABSTRACT

1 Introduction

The complement cascade is an essential part of the innate immune system, comprising over 50 soluble and membrane-bound proteins that work together to destroy pathogens and maintain tissue homeostasis by removing dying cells (1). It involves three distinct pathways: the classical, alternative and lectin pathway. All rely on different molecules for initial cascade activation, yet they converge to a central step where the C3 convertase cleaves complement component C3 into the anaphylatoxin C3a and the opsonin (i)C3b. Invading microorganisms and dead cells become opsonized by (i)C3b, which enables phagocytic cells to recognize and internalize them. Depending on the nature of the dying cell, diverse molecules may facilitate clearance. For instance, apoptotic bodies unveil 'eat me' signals on their membranes, in particular phosphatidylserine, which is recognized by a multitude of phagocytic receptors on leukocytes (2). Complement also contributes to this removal via binding of C1q to the apoptotic cell, thereby opsonizing it and activating the complement pathway to facilitate clearance (3, 4). Even though the general role of (i)C3b in phagocytosis is well-established, so far nearly all research on complement-mediated phagocytosis focused on microorganism clearance and efferocytosis (of apoptotic cells) (5–8). The removal of cellular corpses resulting from necrosis, referred to as necrotic cell debris, has been largely overlooked both in terms of mechanism description and physiological impact *in vivo*.

Necrotic cell death diverges morphologically and immunologically from apoptosis due to plasma membrane rupture, the spilling of intracellular contents into the surrounding tissue, and the subsequent inflammatory response (9). These contents serve as damage-associated molecular patterns (DAMPs), which include ATP (10), high-mobility group box 1 (11), actin (12), mitochondria-derived molecules (13) and DNA (14), among others, and will interact with cognate pattern-recognition receptors (PRRs) on immune cells. For example, during drug-induced liver injury, widespread hepatocyte necrosis results in substantial DNA release from necrotic cells and causes intense TLR9-dependent inflammation (15, 16). Other DAMPs such as histones and F-actin released from necrotic cells also contribute heavily to immune responses through Clec2d and Clec9a recognition, respectively (17, 18). These highlight the importance of limiting the accumulation of debris/DAMPs in conditions where necrosis is prominent, such as drug-induced liver injury, atherosclerosis, stroke, severe trauma, and burn injuries.

Phagocytosis is a cellular process of recognition and ingestion of particles larger than 0.5 μm, which promotes tissue homeostasis and elimination of microorganisms. Phagocytes recognize targets through specialized surface receptors, including non-opsonic receptors such as Dectin-1, Mincle, CD14 and CD36, which detect conserved

molecular patterns, as well as various opsonic receptors. Complement receptors [e.g. CR1, CR3 (CD11b/CD18), CR4] are typical phagocytic receptors recognizing particles bound by complement opsonins (19). In general, complement has been implicated in the processing and removal of self-antigens, since the clearance of apoptotic cells is dependent on opsonization by C1q and C3 (20, 21) and complement deficiencies increase the susceptibility to autoimmune disorders (22). Even though the role of complement in the clearance of apoptotic cells is clear, its contribution to the clearance of necrotic cells is poorly understood, with *in vivo* evidence lacking. Our group has recently shown that natural IgM and IgG antibodies are essential for the clearance of necrotic debris *in vivo* (23). Considering the substantial capacity of antibodies to initiate complement, the contribution of complement activation to necrotic cell debris clearance may be central. Therefore, we investigated complement activation in response to necrotic injury in mouse models of drug-induced liver injury and focal thermal injury (FTI) of the liver. We used intravital microscopy (IVM) to unveil the participation of complement in the clearance of necrotic debris *in vivo* and assessed its impact on the recovery from liver injury.

2 Materials and methods

2.1 Mice

8-12 weeks old male and female C57BL/6J and C57BL/6NRj mice were purchased from Janvier Labs. Rag2$^{-/-}$ mice (C57BL/6N-Rag2Tm1/CipheRj) were bred in specific pathogen-free (SPF) conditions at the Animal Facility of the Rega Institute (KU Leuven). C3$^{-/-}$ mice (B6.129S4-C3tm1Crr/J) and Itgam$^{-/-}$ mice (B6.129S4-Itgamtm1Myd/J) were purchased from The Jackson Laboratory. Mice were housed in acrylic filtertop cages with an enriched environment (bedding, toys and small houses) and kept under a controlled light/dark cycle (12/12h) at 21°C with water and food provided *ad libitum*. All experiments were approved and performed following the guidelines of the Animal Ethics Committee from KU Leuven (P125/2019).

2.2 APAP-induced liver injury model

Mice were starved for 15h and given a single oral gavage of 600 mg/kg APAP (Sigma-Aldrich) dissolved in warm PBS. Administration via oral gavage reflects the typical route of APAP-induced liver injury in patients. After 24, 48 or 72h, mice were sacrificed under anesthesia containing 80 mg/kg ketamine and 4 mg/kg xylazine, whereafter liver and blood were harvested. ALT in serum was determined with a kinetic enzymatic kit (Infinity, Thermo Fisher Scientific) according to the manufacturer's instructions.

2.3 C3 ELISA

Serum levels of mouse C3 were determined by a commercially available C3 ELISA kit (ab157711, Abcam) according to the manufacturer's instructions.

2.4 Neutrophil purification

Human neutrophils were purified from whole blood of healthy volunteers by immunomagnetic negative selection (EasySep™ Direct Human Neutrophil Isolation Kit, StemCell Technologies) according to the manufacturer's instructions. Ethical permission for use of human blood-derived leukocytes was obtained with the ethical committee from the University Hospital Leuven (UZ Leuven, S58418). Mouse bone marrow neutrophils were extracted from femurs and tibias of C57BL/6J mice by flushing the bones with 5 ml cold RPMI-1640 medium using a 26-gauge needle. Cells were filtered through a 70 µm nylon strainer and further purified with the EasySep™ mouse neutrophil enrichment kit (StemCell Technologies), following the manufacturer's instructions.

2.5 Histopathology

Liver sections were stained with hematoxylin and eosin (H&E) and used to estimate hepatic necrosis via measurement of the necrotic area in the images. The livers were washed with 0.9% NaCl and fixed in 4% buffered formalin. Subsequently, the samples were dehydrated in ethanol solutions, bathed in xylol and included in histological paraffin blocks. Tissue sections of 5 µm were obtained using a microtome and stained with H&E. Sections were visualized using a BX41 optical microscope (Olympus) and images were obtained using the Moticam 2500 camera (Motic) and Motic Image Plus 2.0ML software.

2.6 Cryosection immunostaining for C3b, C1q, Ki67, fibrin(ogen) and IgM

The left liver lobes of mice were harvested, embedded in Tissue-Tek O.C.T. Compound (Sakura Finetek Europe) and snap frozen in liquid nitrogen. 10 µm sections were cut using a Cryostat Microm CryoStar and subsequently fixed, permeabilized and blocked. Sections were incubated overnight at 4°C with 10 µg/ml polyclonal rabbit anti-human/mouse fibrin(ogen) (Dako), 5 µg/ml rat anti-mouse C3b/iC3b (clone 3/26, Hycult Biotec) and 5 µg/ml rabbit anti-mouse C1q (clone 4.8, Abcam). Secondary antibodies were added for 3h at RT: Alexa Fluor 647 donkey anti-rabbit, Rhodamine RED-X (RRX) donkey anti-mouse IgM, Alexa Fluor 488 donkey anti-rat, Alexa Fluor 560 donkey anti-rabbit (all at 10 µg/mL, Jackson ImmunoResearch). 10 µg/ml of Hoechst was added for 30 min at RT to stain nuclei. Finally, slides were mounted with ProLong Diamond Antifade Mountant. Images were captured using the Andor Dragonfly High-Speed Confocal Microscope (Oxford Instruments) or a Zeiss Axiovert 200M fluorescence microscope, and analyzed with FIJI. 8 images were acquired per liver with a 25X objective. Stained areas were selected using the threshold tool in FIJI, from which the percentage area of staining was determined. Pearson's coefficient was calculated in FIJI using the JACoP plugin. Comparisons between WT and Rag2$^{-/-}$ mice were normalized to the degree of injury [% of fibrin(ogen) labeling]. All images can be provided in different colors upon request.

2.7 Confocal intravital microscopy

Mice were anaesthetized with a subcutaneous injection of 80 mg/kg ketamine and 4 mg/kg xylazine. For the experiments with APAP-induced liver injury, fluorescent antibodies (4 µg/mouse) and dyes (2 µl of a 10 mM Sytox Green solution; Thermo Fisher Scientific) were dissolved in 100 µl sterile PBS and injected intravenously 10 minutes before the surgery. The surgical procedure is described in detail in Marques et al. (24). For the FTI experiments, 1 mm^3 burns were made with a cauterizer and the injury site was then stained with 10 µl of pHrodo Red succinimidyl ester (SE) (4 µM; Thermo Fisher Scientific). The incision was stitched, and after 6h, mice were again anaesthetized with ketamine and xylazine to image the burn injury site. Images were taken every 30 sec for at least 30 min with the Dragonfly Spinning-Disk Confocal Microscope (Oxford Instruments) using the 25X objective. Quantification of phagocytosis was done in a blind manner by two individuals and counted manually. The percentage of Sytox Green labeling was determined from 2 mosaic images, each composed of 16 images per mouse, with FIJI software using thresholding. The % of $CD11b^+$ cells containing DNA was determined using Imaris software. Surfaces overlaying live cells and DNA debris were generated from 3D images and counted manually.

2.8 *In vitro* phagocytosis

Necrotic debris was generated from HepG2 cells by inducing mechanical disruption with a pellet mixer for 5 min in 0.1 M sodium bicarbonate (pH 8.5). The necrotic debris was labeled by adding 2 µl of 10 mM pHrodo Red SE (Thermo Fisher Scientific) solution per $10x10^6$ cells. The debris was opsonized with 20% normal human serum, C1q-depleted serum (Complement Technology) or C3-depleted serum (Complement Technology) in PBS for 1h at 37°C. Opsonized debris was added to purified neutrophils in a 1:10 cell/debris ratio. Neutrophils were stimulated with 10^{-7} M N-formyl-Met-Leu-Phe (fMLF; Sigma-Aldrich) for human neutrophils or 1 µM WKYMVM (Phoenix Pharmaceuticals) for mouse neutrophils, and labeled with 1 µM calcein AM viability dye (Invitrogen). Two 3D mosaics are captured per well, each comprising 9 overlapping images taken after 3h incubation at 37°C with the 25X objective of the Dragonfly Confocal Microscope (Oxford Instruments). Each condition was plated in duplicate and replicated at least 3 times. 3D reconstructions were generated using Imaris software. Additionally, with Imaris, surfaces were overlaid onto live cells and necrotic debris through thresholding, after which the volume of overlap was calculated in $µm^3$.

2.9 Flow cytometry

Liver lobes were surgically removed, put in MACS tubes with RPMI-1640 (Biowest Riverside) and minced with a gentleMACS Dissociator (Miltenyi Biotec). To this suspension, 2.5 mg collagenase D (Roche) and 1 mg DNAse I were added per liver for 1h at 37°C. The cell suspension was washed with PBS (300 g, 5 min, 4°C). Non-parenchymal cells were separated by density gradient centrifugation at 60 g for 3 min at 4°C. Supernatant was collected and filtered through a 70 µm nylon cell strainer. After centrifugation (300 g, 5 min, 4°C), ACK Lysing buffer (Gibco) was added for 10 min to the pellet to lyse red blood cells. $1x10^6$ cells were collected in FACS tubes and washed with PBS (300 g, 5 min, 4°C). Zombie Aqua Fixable Viability dye (Biolegend) together with mouse FcR blocking Reagent (Miltenyi Biotec) were incubated for 15 min in the dark. Then, cells were washed with PBS supplemented with 0.5% bovine serum albumin (BSA) and 2 mM EDTA and the fluorescently labeled antibodies were incubated for 25 min at 4°C in the dark. After a final washing step, cells were read in a Fortessa X20 (BD Biosciences). Data was analyzed using FlowJo 10.8.1 software.

2.10 RNA extraction from human neutrophils fed necrotic debris

HepG2 cells were mechanically lysed using a 22G syringe in PBS with 20 µg/ml RNAse A (Sigma-Aldrich) to generate RNA-free necrotic debris. The debris was incubated for 30 min at 37°C to allow enzyme activity. Then, the debris was washed twice with PBS containing 2 mM EDTA and 0.1% BSA, and centrifuged at 60g for 3 min to remove intact cells. The debris was opsonized with 20% serum or C3-depleted serum (Complement Technology) and then incubated for 1h at 37°C. Neutrophils from healthy donors were purified by immunomagnetic negative selection with an EasySep kit and stimulated with 10^{-7} M fMLF. Cells and debris were co-incubated in a 6 well plate at a 1:10 cell/debris ratio and centrifuged at 300g for 5 min before being incubated for 3h at 37°C. Cells were harvested and total RNA was extracted by lysing the cells with β-mercaptoethanol and a Rneasy Plus Mini Kit (Qiagen) following the manufacturer's instructions. After extraction, total RNA quality and quantity were determined using a Nanodrop.

2.11 qPCR

cDNA was obtained by reverse transcription using the high-capacity cDNA Reverse Transcriptase kit (Applied Biosystems). mRNA levels were analyzed by quantitative PCR using a TaqMan Gene Expression Master Mix (Applied Biosystems) and a 7500 Real-Time PCR System apparatus. Expression levels of genes of interest were normalized for the average RNA expression of three housekeeping genes (CDKN1A, 18S and GAPDH) using the $2^{-\Delta\Delta CT}$ method (25).

2.12 Statistical analysis

Data were analyzed using GraphPad Prism v9.3.1. All data are expressed as mean ± standard error of the mean (SEM). A Shapiro-Wilkinson test was performed to check for normality. Normally distributed data were analyzed with a Student's t test or One-way ANOVA. Non-parametric data were analyzed with a Mann-Whitney test or Kruskal-Wallis test. Grubb's test (extreme

studentized deviate) was applied to determine significant outliers, which are identified as red dots in the graphs and removed from statistical analysis. A p-value equal or lower than 0.05 was considered significant.

3 Results

3.1 Complement proteins C1q and (i)C3b are deposited at sites of necrotic liver injury

To assess complement activation at necrotic injury sites, a mouse model of paracetamol/acetaminophen (APAP)-induced liver injury was used, as it is characterized by extensive death of hepatocytes through necrosis (16). A sublethal dose of 600 mg/kg APAP was administered via oral gavage, causing significant liver damage as early as 12h after administration. In this acute model, hepatocellular necrosis was observed by elevated levels of serum alanine aminotransferase (ALT) (Supplementary Figure S1A), an enzyme primarily found in hepatocytes that serves as a biomarker for liver damage. Using histopathology, necrotic lesions were detected around the centrilobular veins, a typical pattern for APAP-induced injury, with the highest severity 12h after APAP administration (Supplementary Figures S1B, C). At 48h, the injury decreased significantly, as depicted by lower serum ALT levels and reduced necrotic areas (Supplementary Figures S1A, B). Fibrin deposition, known for its specific accumulation at necrotic sites after the activation of the coagulation cascade (26), was evaluated over time on liver cryosections to estimate the area of necrosis. Significant fibrin (ogen) staining was observed after 24h, whereafter it gradually decreased (Figures 1A, C; Supplementary Figure S2A). A similar pattern was observed for IgM, with the highest deposition occurring after 24h and diminishing at later timepoints (Figures 1B, D; Supplementary Figure S2B). Remarkably, C1q and (i)C3b deposition remained high up to 48h (Figures 1E, F), indicating that the deposition of antibodies preceded complement activation through C1q binding and C3 cleavage. The staining in necrotic regions was not because of autofluorescence or unspecific labeling as confirmed in cryosections stained with secondary antibodies only (Supplementary Figure S1D). Pearson's correlation coefficient between (i)C3b and fibrin was significantly higher in comparison to (i)C3b and intact cell nuclei in the liver (Figure 1G). In addition, the other components of the classical complement pathway, IgM and C1q, also had high colocalization with (i)C3b (Figure 1H). All this shows that complement proteins are deposited specifically at sites of necrotic injury in the liver. These data were supported by significantly lower C3 levels in the serum of APAP-treated mice (Figure 1I), which confirm complement activation in response to injury.

3.2 $C3^{-/-}$ mice have delayed recovery from liver injury

To investigate the contribution of C3 to the resolution of necrotic liver damage, $C3^{-/-}$ mice were subjected to APAP overdose and evaluated at 2 timepoints: a) after 24h, to assess the peak of injury and b) after 48h, to observe the degree of tissue repair. No differences in serum ALT levels were observed after 24h, while significantly higher levels of ALT were found after 48h in $C3^{-/-}$ mice compared to WT mice (Figure 2A). In addition, fibrin staining of liver cryosections revealed no differences at the peak of injury, whereas more fibrin staining was found in $C3^{-/-}$ mice at the later timepoint (Figure 2B), indicating that C3 deficiency leads to larger, unresolving necrotic areas in the liver. During the liver regeneration phase, cellular proliferation can be estimated by the expression of Ki67 in liver cryosections. Using this approach, we observed a significant decrease in cell proliferation in $C3^{-/-}$ mice 48h after APAP overdose (Figure 2C), confirming that the absence of C3 impairs liver regeneration and recovery from injury.

To directly assess whether C3 deficiency affects the amount of necrotic debris in injured tissues, we performed confocal IVM of mouse livers. Considering that DNA is abundantly released by necrotic hepatocytes (16) and based on the observed differences during the resolution phase (Figures 2A-C), we chose to measure the amount of DNA exposed in the liver 48h after the APAP challenge using the membrane-impermeable DNA dye Sytox Green. Interestingly, WT mice presented minimal extracellular DNA in the liver at the 48h timepoint, which is consistent with the removal of necrotic debris and tissue recovery at that phase (Figures 2D, E). Moreover, the vast majority of the fluorescent signal observed in the images of WT mice consisted of background fluorescence from healthy hepatocyte nuclei (Figure 2D). In contrast, $C3^{-/-}$ mice had significantly more extracellular DNA debris, demonstrating that these mice have a clear defect in the removal of necrotic debris from the liver (Figures 2D, E). These results link poor recovery from liver injury in $C3^{-/-}$ mice to impaired clearance of necrotic cell debris.

3.3 Phagocytosis of necrotic DNA debris depends on complement activation

To explore how debris persisted in injury sites, an analysis of the recruited leukocytes and their ability to take up debris was performed. The inflammatory response triggered by liver injury led to the recruitment of $CD11b^+$ leukocytes to necrotic areas identified by the extracellular DNA staining (Figure 3A, **upper panels**). These cells consisted primarily of inflammatory monocytes ($CCR2^+$), neutrophils ($Ly6G^+$) and macrophages ($F4/80^+$) (Figure 3A, lower panels; Supplementary Figures S3A-C). Of interest, CD11b, the α_M subunit of the complement receptor CR3 (CD11b/CD18), which is known for its involvement in complement-mediated phagocytosis, was increased in neutrophils and monocytes during liver injury (Supplementary Figures S3D-F). Besides CD11b+ leukocytes, other immune cells (DCs, T and B cells) are present in lower percentages in the injured liver (Supplementary Figure S3G). However, their role in debris phagocytosis is less anticipated and therefore not examined in this study. We then inquired whether $CD11b^+$ cells were able to internalize extracellular DNA debris using IVM. Numerous $CD11b^+$ leukocytes were visualized deep within necrotic areas

10.3389/fimmu.2024.1512470

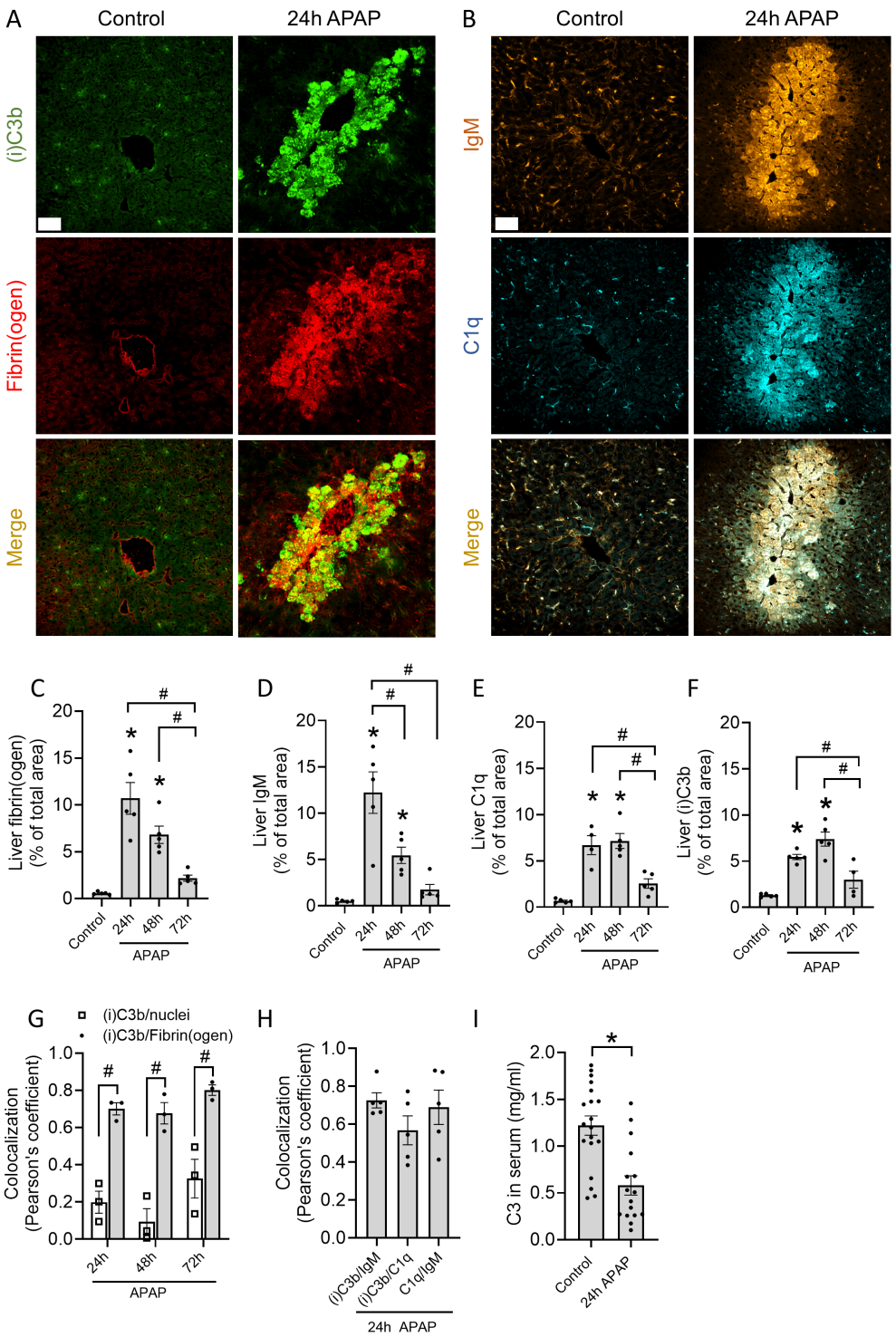

FIGURE 1
Complement proteins C1q and (i)C3b are deposited at sites of necrotic liver injury. **(A, B)** Representative immunofluorescence images of liver cryosections from control mice or mice challenged with acetaminophen (APAP; 600 mg/kg) for 24h. Green: (i)C3b; red: fibrin(ogen); Orange: IgM; Cyan: C1q. Scale bar represents 50 µm. **(C-F)** Quantifications of the area percentage stained with fibrin(ogen) **(C)**, IgM **(D)**, C1q **(E)** and (i)C3b **(F)** in liver cryosections of control mice and mice 24, 48 or 72h after receiving an APAP overdose. **(G)** Pearson's correlation coefficient of (i)C3b and nuclei (Hoechst) or fibrin(ogen) in the injured livers 24, 48 and 72h after APAP overdose. **(H)** Pearson's correlation coefficient between (i)C3b, IgM and C1q in the injured livers 24h after APAP overdose. **(I)** C3 levels in the serum of control mice or challenged with APAP for 24h. Image quantifications were pooled from 8 fields of view. Each dot represents a single mouse. At least 4 mice were used per group. Data are represented as mean ± SEM. *p ≤ 0.05 compared to control; #p ≤ 0.05 between indicated groups. APAP, acetaminophen; MFI, Mean fluorescence intensity.

10.3389/fimmu.2024.1512470

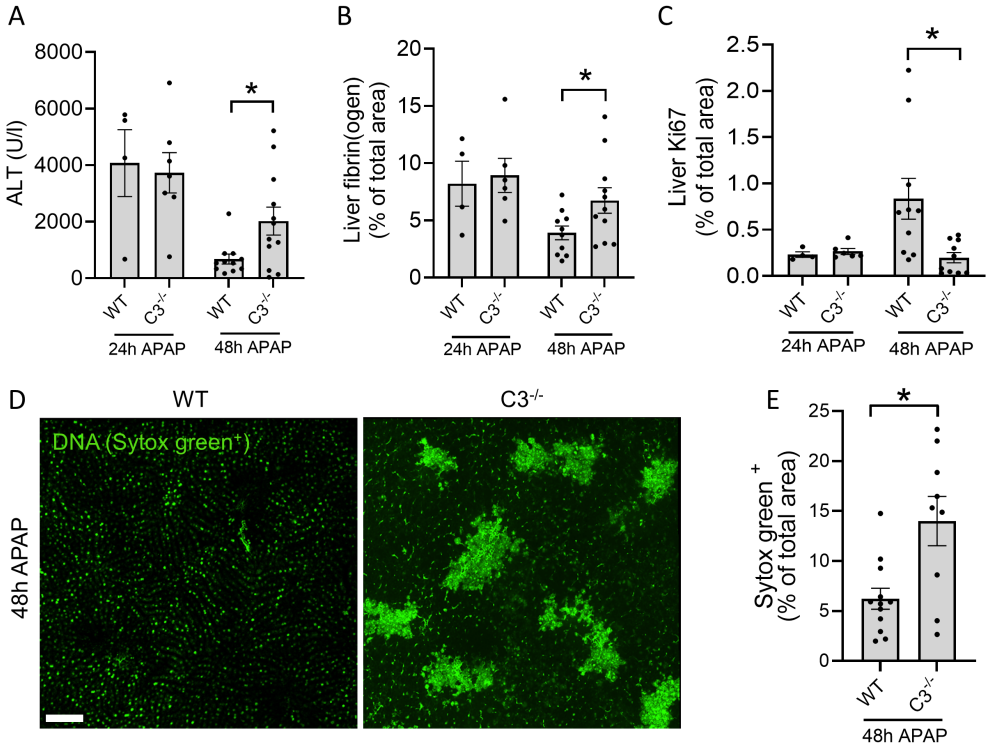

FIGURE 2
$C3^{-/-}$ mice have delayed recovery from liver injury. **(A)** Serum ALT levels in WT and $C3^{-/-}$ mice 24 and 48 hours after APAP overdose. **(B)** Quantification of area fraction stained with fibrin(ogen) in liver cryosections. **(C)** Quantification of area fraction stained with Ki67 in liver cryosections of APAP-challenged WT and $C3^{-/-}$ mice. **(D)** Representative confocal IVM images of WT and $C3^{-/-}$ mice showing the deposition of DNA (Sytox Green^{+}) in the liver 48 hours after APAP overdose (600 mg/kg). Scale bar represents 200 µm. **(E)** Quantification of Sytox Green labeling in the liver of APAP-challenged WT and $C3^{-/-}$ mice after 48h. The percentage of Sytox Green labeling was determined from 2 mosaic images, each composed of 16 images per mouse taken with the 25X objective, analyzed with FIJI software using thresholding. Each dot represents a single mouse. At least 4 mice were used per group. Data are represented as mean ± SEM. *$p \leq 0.05$ between indicated groups. APAP, acetaminophen; ALT, alanine aminotransferase.

using Z-stacks, and multiple cells contained Sytox Green^{+} particles (Figure 3B, Supplementary Video S1). In total, 12% of the CD11b^{+} cells contained DNA particles, with an average of 2 particles per cell (Figures 3C, D). Internalization of DNA debris was confirmed upon intravenous administration of DNAse to remove the bulk of extracellular DNA in necrotic areas. DNA-positive vesicles in CD11b^{+} leukocytes remained after DNAse injection, indicating that the DNA particles were located intracellularly, likely in phagosomes, which are not accessible to the circulating DNAse treatment (Supplementary Figure S3H, Supplementary Video S2).

After observing impaired necrotic DNA removal in $C3^{-/-}$ mice (Figures 2D, E), flow cytometry was performed to quantify DNA uptake by leukocytes in WT and $C3^{-/-}$ mice (see Supplementary Figure S7 for gating strategy). Again, the membrane-impermeable DNA dye Sytox Green was injected intravenously 2h before sacrificing mice that received an APAP overdose 24h prior. This allowed sufficient time for the fluorescently-labeled necrotic DNA to be phagocytosed. We observed that a significantly lower percentage of neutrophils and macrophages were able to internalize DNA debris in the absence of C3, demonstrating that debris clearance depends at least partially on complement opsonization (Figures 3E, F). Importantly, no differences were observed in the number of neutrophils (Ly6G^{+}) and macrophages (Ly6G^{-}/Ly6C^{-}/F4/80^{+}) present in the injured liver between WT and $C3^{-/-}$ mice (Figures 3I, J), suggesting that impaired DNA removal observed in $C3^{-/-}$ mice may be due to the reduced phagocytic capacity of these cells. In contrast, classical and non-classical monocytes did not require C3 to take up DNA debris in the injured liver (Figures 3G, H), suggesting that different leukocyte populations utilize distinct mechanisms for debris clearance. However, the number of classical (Ly6G^{-}/Ly6C^{+}) and non-classical monocytes (Ly6C^{-}/CX_3CR1^{+}) recruited to the injured liver in $C3^{-/-}$ mice was significantly reduced (Figures 3K, L), showing that less monocytes reached the injured liver to perform debris phagocytosis. Overall, these data show that necrotic DNA debris is cleared by leukocytes in the liver and that neutrophils and macrophages require complement opsonization of debris for its uptake.

3.4 Complement opsonization and clearance of necrotic cell debris are not exclusive to drug-induced liver injury

Reduced clearance of DNA debris in the absence of C3 was observed in a model of acute liver injury induced by APAP

10.3389/fimmu.2024.1512470

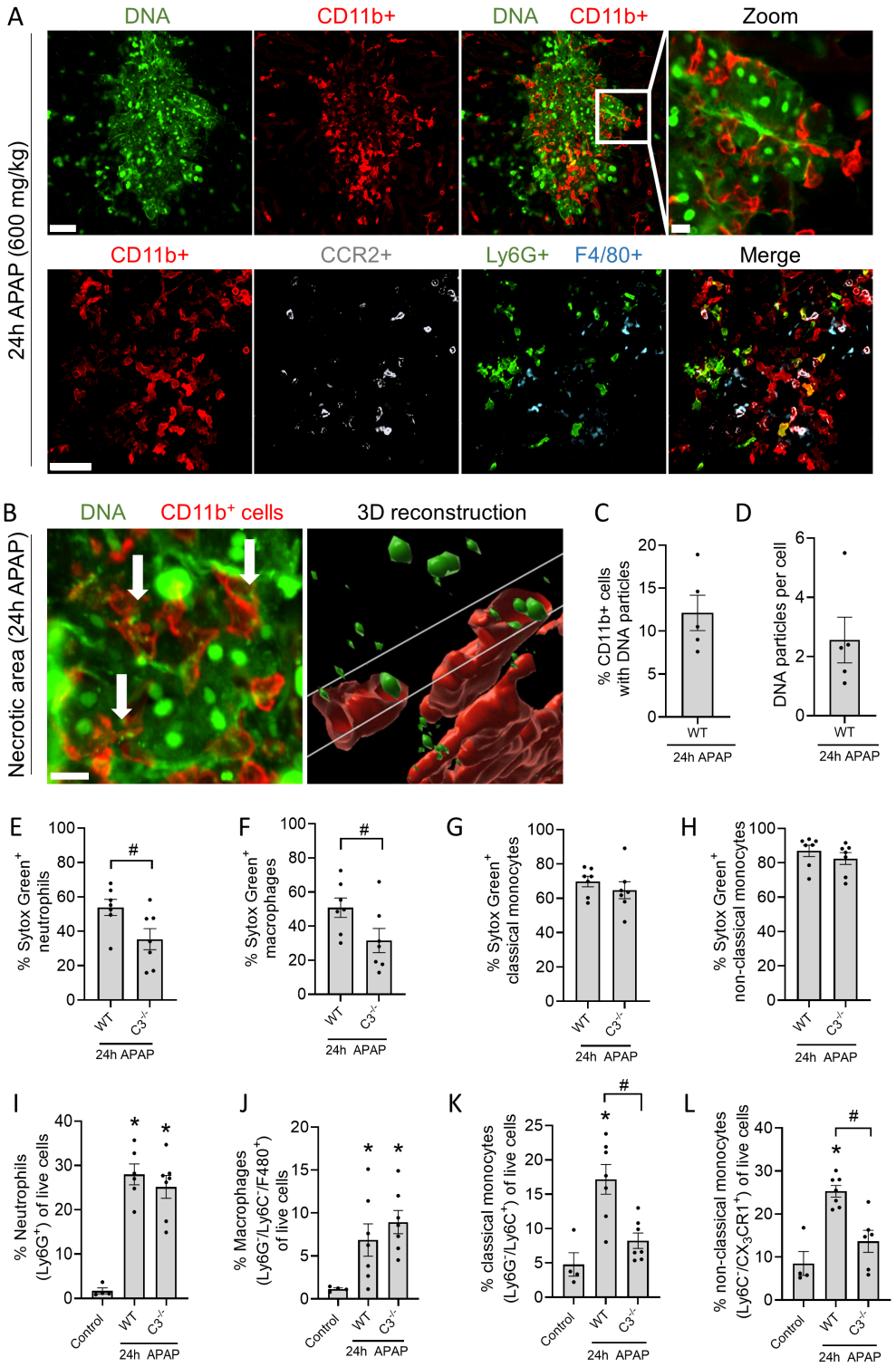

FIGURE 3
Phagocytosis of necrotic DNA debris depends on complement activation. **(A)** Representative confocal IVM images of the injured liver 24h after APAP overdose. Sytox Green (Green; DNA), CD11b (Red; leukocytes), CCR2 (White; monocytes), Ly6G (Green; neutrophils) or F4/80 (Cyan; macrophages). Upper and lower panels are from different experiments. Scale bar represents 50 µm, scale bar zoomed image represents 10 µm. **(B)** Representative confocal IVM image of the injured liver 24h after APAP and an image of a 3D reconstruction with Imaris software. 2 µl of the DNA impermeable dye Sytox Green was injected 1h before imaging. Leukocytes were labeled with anti-CD11b antibody (Red). Scale bar represents 50 µm. **(C)** Percentage of $CD11b^+$ cells containing DNA particles in the injured liver of mice quantified by IVM. **(D)** Average number of DNA particles per $CD11b^+$ cell in the injured liver of mice quantified by IVM. **(E-L)** Flow cytometry of non-parenchymal cells identifying the percentage of neutrophils ($Ly6G^+$), non-classical monocytes ($Ly6C^-/CX_3CR1^+$), classical monocytes ($Ly6G^-/Ly6C^+$) and macrophages ($Ly6G^-/Ly6C^+/F4/80^+$) in the injured liver and the percentage of those leukocytes containing extracellular DNA (Sytox Green+). The cell-impermeable DNA dye Sytox Green was injected 2h before harvesting the liver of control, WT and $C3^{-/-}$ mice that received an APAP overdose 24h prior. Data are represented as mean ± SEM. Each dot represents a single mouse. At least 4 mice were used per group. *p ≤ 0.05 compared to control; #p ≤ 0.05 between indicated groups. APAP, acetaminophen.

overdose. To validate whether this finding applies to other types of injuries, we investigated debris clearance in a model of focal thermal injury (FTI) of the liver. In this model, necrotic lesions are induced locally with a hot needle, facilitating the observation of phagocytosis *in vivo*. This was challenging in the APAP model due to widespread necrosis throughout the liver causing an abundance of debris. The localized nature of the thermal injury allowed us to label necrotic debris by applying a droplet of the pH-sensitive dye pHRodo Red succinimidyl ester on top of the lesion. This dye binds covalently to proteins and exhibits increased fluorescence when the ingested material is processed in the acidic environment of a phagolysosome.

Our previous work demonstrated that neutrophils predominated in the injured area 6h after FTI, with monocytes being attracted after 12h (23). The entire image of the FTI shows distinct burn injury zones, with neutrophils mostly accumulating around the injury core (Supplementary Figure S4A). Using IVM, neutrophils carrying pHRodo-labeled debris were observed crawling from the injury border into the necrotic core (Figure 4A, Supplementary Video S3). Approximately 75% of neutrophils at the injury site had pHRodo-containing phagosomes, whereas less than 5% of neutrophils in healthy areas of the liver phagocytosed debris (Figure 4B). This finding was confirmed by flow cytometry, which showed a significantly increased MFI of pHRodo in neutrophils and monocytes at the burn injury site compared to leukocytes in healthy areas (Supplementary Figures S4B, C; see Supplementary Figure S7 for gating strategy). Similarly to the APAP model, complement proteins C1q and (i)C3b were specifically deposited on necrotic lesions 6h after FTI (Figure 4C). Both components colocalized with each other and fibrin (Supplementary Figures S4D, E). Quantification of necrotic debris clearance by flow cytometry demonstrated a significant decrease in the percentage of neutrophils and non-classical monocytes phagocytosing debris in $C3^{-/-}$ mice compared to WT (Figures 4D, E). Interestingly, this phenomenon was not observed in classical monocytes nor macrophages (Figures 4F, G). To be noted, the number of neutrophils migrating in the burn injury site (Supplementary Figure S4F), and the percentage of neutrophils, macrophages and non-classical monocytes attracted to the injured liver did not differ between WT and $C3^{-/-}$ mice, while the percentage of classical monocytes was significantly reduced in $C3^{-/-}$ mice (Supplementary Figures S4G-J).

Due to the increase in $CD11b^{+}$ cells in response to liver injury (Supplementary Figures S3D-F) and its known role in complement-mediated phagocytosis, the role of CR3 on debris uptake and liver resolution was investigated. In the FTI, using $CD11b^{-/-}$ mice, we found a significant decrease in debris clearance by neutrophils and non-classical monocytes (Figures 4D, E), while no difference was observed in classical monocytes and macrophages (Figures 4F, G). Moreover, the attracted phagocyte populations at the injury site were not affected by the deficiency in $CD11b^{-/-}$, indicating that the defective clearance is not connected to inhibition of leukocyte recruitment (Supplementary Figures S4F-J). Conversely, no significant effect was observed on the progression of liver injury in $CD11b^{-/-}$ mice or in WT mice that received a CD11b blocking antibody, as evidenced by similar ALT values and fibrin staining (Supplementary Figures S5A-E) after APAP overdose. These data show that in the FTI, neutrophils and monocytes migrate to the necrotic lesion to phagocytose necrotic debris, a process which depends on C3 and CD11b/CD18 for neutrophils and non-classical CX_3CR1^{+} monocytes, whereas classical $CCR2^{+}$ monocytes rely on other unidentified receptors.

3.5 Opsonization controls the volume of debris that is phagocytosed and regulates gene expression in neutrophils

Investigating the factors driving debris phagocytosis *in vivo* is challenging due to the necessity of multiple knock-out strains and the technical limitations associated with observing cellular events in living mice. To overcome this, we developed an *in vitro* phagocytosis assay, enabling us to study the role of specific complement proteins in necrotic debris clearance. This approach also allowed us to verify our findings in human neutrophils and human necrotic debris. In this assay, necrosis was induced by mechanically disrupting HepG2 cells, whereafter sera lacking specific complement components were used to opsonize the debris. Images were taken with a confocal microscope 3h after combining the opsonized necrotic debris with human or mouse neutrophils. Importantly, the HepG2 cell debris itself did not contain detectable levels of C3/(i)C3b, as demonstrated by immunostaining HepG2 debris *in vitro* (Supplementary Figures S6A, B). However, when the debris came in contact with whole serum, it became clearly opsonized by C3/(i)C3b confirming the capacity of debris to induce complement activation.

In vitro engulfment of pHRodo-labeled necrotic debris by live neutrophils was visualized by 3D reconstruction (Figure 5A). Interestingly, the percentage of bone-marrow derived mouse neutrophils that performed phagocytosis did not differ when presented with debris opsonized with serum, serum lacking C3 (from $C3^{-/-}$ mice) or lacking antibodies (from $Rag2^{-/-}$ mice) (Figure 5B). However, the volume of the necrotic debris internalized by neutrophils was significantly reduced when the debris was opsonized with serum lacking C3 (Figure 5C). Likewise, freshly isolated neutrophils from healthy donors showed no difference in phagocytosis rates when debris was opsonized with serum, C1q-depleted serum or C3-depleted serum (Figure 5D). Nevertheless, a significant decrease in the volume of debris uptake was observed when it was opsonized with serum lacking C3 (Figure 5E). Latrunculin served as a positive control, as it inhibits phagocytosis globally by disrupting actin polymerization. These findings underscore the ability of both human and mouse neutrophils to internalize necrotic debris, while highlighting the role of complement on the amount of debris taken up through phagocytosis.

To investigate the impact of debris phagocytosis on gene expression, qPCR was performed on human neutrophils incubated with necrotic debris from HepG2 cells. Neutrophils were exposed to pure unopsonized debris, debris opsonized with normal serum or with C3-depleted serum for 3 hours. The data were normalized to unopsonized debris in order to account for stimulation by DAMPs present in necrotic cell debris. Interestingly, uptake of serum-opsonized debris induced the upregulation of *PTGS2* (encoding COX2) in neutrophils (Figure 5F). COX2 is an enzyme with dual role in inflammation, catalyzing the production

10.3389/fimmu.2024.1512470

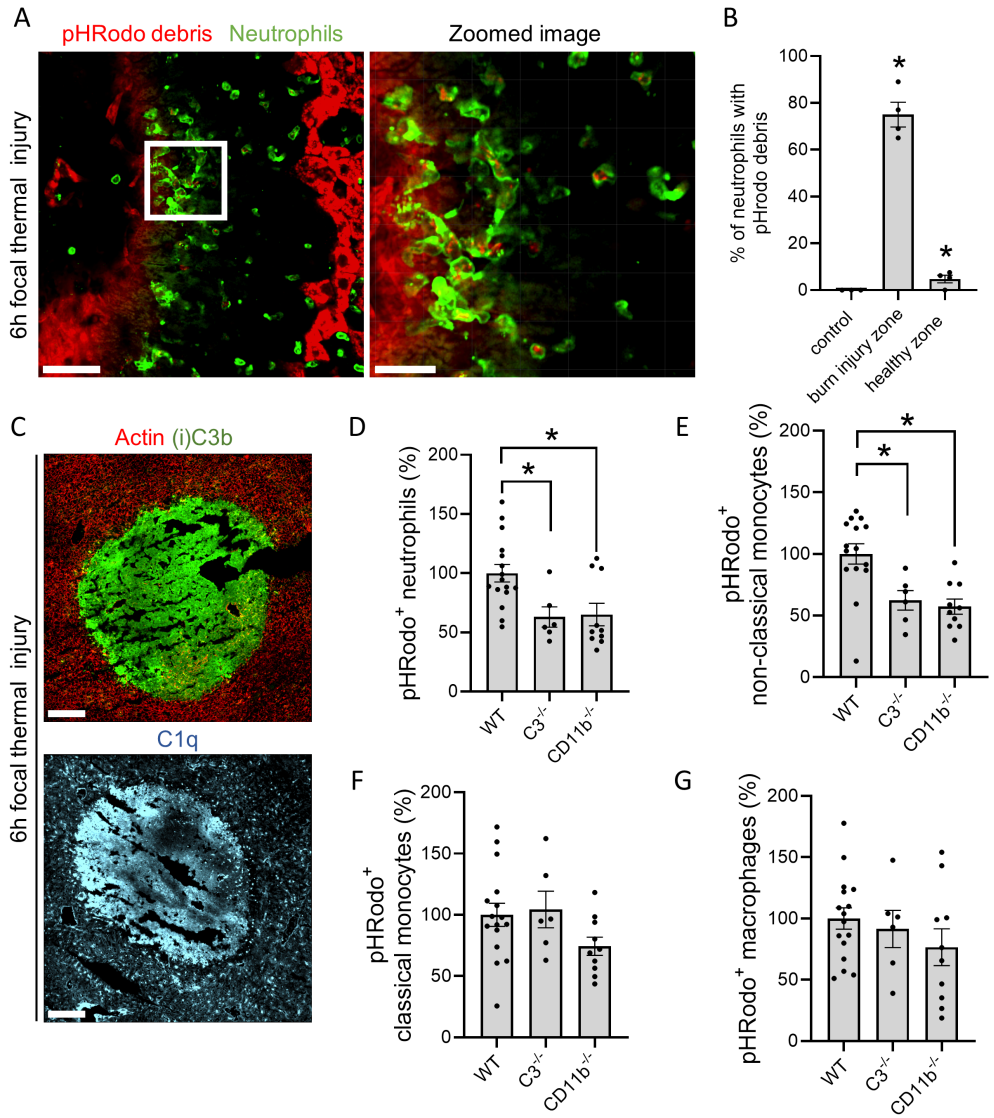

FIGURE 4
Complement opsonization and clearance of necrotic cell debris are not exclusive to drug-induced liver injury. **(A)** Representative confocal image of neutrophils (Ly6G; green) and necrotic debris (pHRodo; red) in the liver 6h after FTI. pHRodo-SE was applied on top of the lesion 6h before imaging. Scale bar represents 50 µm, scale bar zoomed image represents 20 µm. **(B)** Quantification of the percentage neutrophils carrying pHRodo labeled debris at different areas of the injury. **(C)** Representative immunofluorescence stainings of liver cryosections 6h post burn injury. Green: (i)C3b; Cyan: C1q. Scale bar represents 200 µm. **(D-G)** Flow cytometry of non-parenchymal cells isolated from liver FTI sites showing the percentage **(D)** pHrodo$^+$ neutrophils (Ly6G$^+$), **(E)** pHrodo$^+$ non-classical monocytes (Ly6C$^-$/CX$_3$CR1$^+$), **(F)** pHrodo$^+$ classical monocytes (Ly6C$^+$/CX$_3$CR1$^-$/CCR2$^+$) and macrophages (F4/80$^+$). Data are represented as mean ± SEM. Each dot represents a single mouse. At least 3 mice were used per group. *p ≤ 0.05 compared to WT.

of pro-inflammatory prostaglandins from arachidonic acid, such as PGE2, but also participating in the synthesis of numerous pro-resolving lipid mediators (27). *PTGS2* upregulation was reversed when the debris was opsonized with serum lacking C3, indicating a direct effect of complement on the upregulation of COX2, which was already observed for monocytes but not neutrophils (28). *CXCR2*, coding for a major chemokine receptor in neutrophils that promotes both chemotaxis and reverse migration (29, 30) was also upregulated by incubation with opsonized debris. Moreover, in the absence of C3, CXCR2 expression levels returned to baseline (Figure 5G). In addition, incubation with opsonized debris led to the expression of other immunoregulatory and pro-resolving genes in neutrophils, namely, *CXCR4*, encoding a chemokine receptor associated with homing of neutrophils to the bone marrow for apoptosis and removal (31, 32); the immunoregulatory cytokine *IL10*, and *ANXA1*, encoding the protein annexin A1 that dampens leukocyte chemotaxis, respiratory burst and phagocytosis (Figures 5H-J) (33). The absence of C3 in the serum significantly reduced the expression of *CXCR4*, *IL10 or ANXA1*, indicating the essential role of C3 opsonization in the induction of pro-resolving genes in neutrophils. Moreover, alterations in gene expression in neutrophils are specific, since multiple genes were unaffected by stimulation with opsonized debris, including *ALOX5, CYBB, CASP3, ARG1, FPR1* and *FPR2* (Supplementary Figures S6C-H).

Overall, the gene expression induced by the clearance of opsonized necrotic debris reflects a pro-resolving response in neutrophils, which is C3-dependent and plays a central in promoting tissue repair.

3.6 Classical complement pathway is activated in response to necrotic debris

Lastly, we investigated whether the classical complement pathway contributed to (i)C3b opsonization of necrotic debris. For this, Rag2$^{-/-}$ mice, which lack mature T and B cells and therefore also antibodies, were subjected to the APAP overdose. Activation of the classical complement pathway requires the association of C1q with target-bound IgM or multiple IgGs, thus, this complement pathway cannot be activated in Rag2$^{-/-}$ mice. First, the absence of IgM was confirmed by immunostaining, which revealed that IgM labeling in the injured Rag2$^{-/-}$ liver was essentially absent (Figures 6A, D, E). Interestingly, 24h after APAP overdose, liver cryosections showed significantly increased fibrin deposition in Rag2$^{-/-}$ mice compared to WT mice (Figures 6B, C). In our previous work, the absence of antibodies was shown to be responsible for a delayed liver resolution

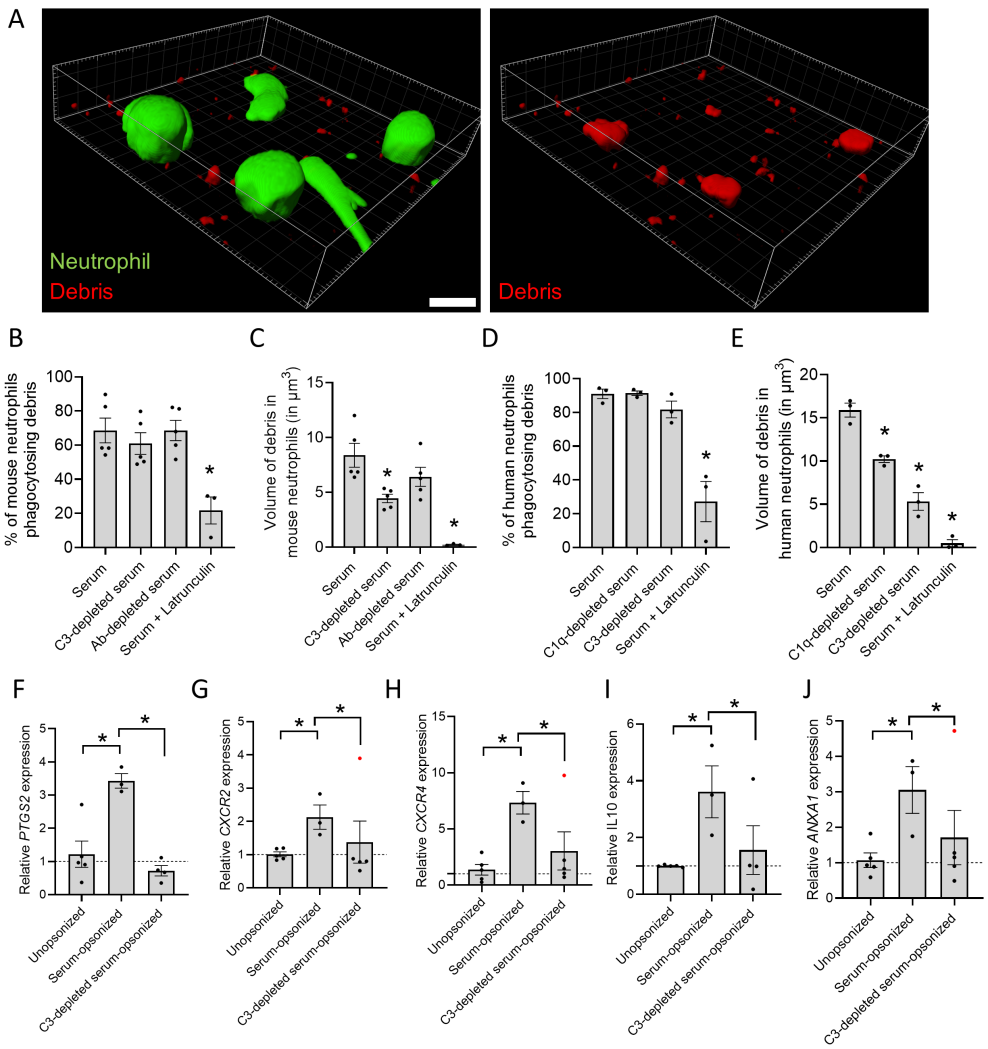

FIGURE 5
Opsonization controls the volume of debris phagocytosed and regulates gene expression in neutrophils. **(A)** 3D reconstruction with Imaris software of image of human neutrophils stained with Calcein (green) phagocytosing pHrodo-labeled necrotic debris (red). Scale bar represents 10 µm. **(B)** Percentage of bone-marrow derived mouse neutrophils phagocytosing necrotic debris opsonized with serum, C3-depleted serum (from C3$^{-/-}$ mice) or antibody-depleted serum (from Rag2$^{-/-}$ mice). **(C)** Volume of necrotic debris phagocytosed by bone-marrow derived mouse neutrophils which was opsonized with serum, C3-depleted serum or antibody-depleted serum. **(D)** Percentage of human neutrophils phagocytosing necrotic debris opsonized with serum, C1q-depleted serum or C3-depleted serum. **(E)** Volume of necrotic debris phagocytosed by human neutrophils which was opsonized with serum, C1q-depleted serum or C3-depleted serum. **(F-J)** Gene expression of human neutrophils incubated with unopsonized, serum-opsonized or C3-depleted serum-opsonized human necrotic debris. Data are normalized to the average expression of 3 housekeeping genes (GAPDH, 18s and CDKN1A) and represented as $2^{-\Delta\Delta Ct}$ relative to the unopsonized group. 10 µM latrunculin is used as a negative control. Data are represented as mean ± SEM. Each dot represents an independent experiment. Significant outliers are indicated as red dots. *p ≤ 0.05 compared to serum group or between indicated groups.

due to impaired necrotic debris clearance (23). Because the degree of necrotic injury also affects the degree of C1q and (i)C3b deposition, complement immunostaining was normalized to the area of fibrin staining. With this approach, we observed no difference in C1q binding to necrotic areas in Rag2$^{-/-}$ mice compared to WT (Figure 6F). Similarly, the mean fluorescence intensity (MFI) of C1q was not different between WT and Rag2$^{-/-}$ mice, indicating that C1q binding does not rely on antibody opsonization of necrotic debris (Figure 6G). However, the area of (i)C3b deposition was significantly decreased in Rag2$^{-/-}$ mice, with also significantly lower MFI in (i)C3b-stained areas (Figures 6H, I), even though it has been shown that Rag2$^{-/-}$ mice have elevated C3 levels in blood (34). These data indicate that loss of IgM and IgG antibodies diminishes the level of complement activation on necrotic sites, even though C1q binding remains unaffected. These data also demonstrate that the classical complement pathway is activated in response to necrotic debris, leading to (i)C3b deposition in injury sites.

4 Discussion

We observed specific deposition of C1q and (i)C3b at necrotic lesions in the liver, in line with previous literature (Figure 1) (35–37). We also demonstrated that in the absence of antibodies IgM and IgG, complement protein C1q still bound necrotic debris (Figure 6), likely due to its interaction with various ligands which include histones, DNA, C-reactive protein, pentraxin 3 and serum amyloid P component (4, 38–40). Interestingly, the absence of antibodies significantly reduced C3b deposition, even though Rag2$^{-/-}$ mice have elevated C3 levels compared to WT mice (34). This suggests that C3b deposition on necrotic lesions relies, at least partially, on the classical complement pathway, which is hampered in the absence of antibodies despite C1q presence. An *in vitro* study corroborated this, since adding C1q to sera lacking IgM and C1q did not affect C3 deposition on apoptotic cells (41). Of course, the activation of the alternative and lectin complement pathway in response to necrotic cells should not be overlooked, as properdin, a positive regulator of the complement system, has been proven to bind to necrotic cells and activate the alternative pathway (42). Also, mannose-binding lectin was shown to interact with apoptotic and necrotic cells and to facilitate uptake by macrophages *in vitro* (43). Realization that the classical pathway is activated reveals additional opportunities to ameliorate debris clearance. Patients with severe necrotic injuries might benefit from intravenous immunoglobulin (IVIG) supplementation and blood transfusions. The administered natural antibodies may bind necrotic debris, triggering C3 cleavage via the classical pathway, and aiding in the clearance of debris. Moreover, our previous work showed that the supplementation of natural antibodies directly enhanced Fc receptor-mediated phagocytosis, meaning that debris would be cleared via both complement- and Ab-mediated phagocytosis (23).

Evaluating liver injury in C3$^{-/-}$ mice following APAP overdose showed us a delayed recovery and the prolonged accumulation of necrotic debris (Figure 2). Roth et al. observed lower serum ALT levels in C3$^{-/-}$ mice 6 and 12h post-APAP, possibly due to the administration of a lower dose of 300 mg/kg APAP intraperitoneally and the shorter evaluation time (35). However, other studies have similarly noted impaired liver regeneration in C3$^{-/-}$ mice after toxic-injury induced by CCl_4 and partial hepatectomy (44, 45). Although impaired liver resolution and debris accumulation in C3$^{-/-}$ mice could be explained by impaired debris phagocytosis, other factors also contribute to this worsened phenotype. The absence of anaphylatoxins C3a and C5a impact liver regeneration by affecting hepatocyte priming and inhibiting neutrophil and monocyte chemotaxis (41, 46, 47). In addition to the decreased presence of monocytes at the injury site to perform debris phagocytosis, the reduced differentiation into monocyte-derived macrophages also contributes to delayed injury resolution, as observed in CCR2$^{-/-}$ mice (48, 49). The absence of the C3a/C3aR axis may also influence CCL2 expression in leukocytes, potentially affecting monocyte infiltration into the injured liver in C3$^{-/-}$ mice. This is supported by studies showing that C3a upregulates CCL2 expression in human keratinocytes and mast cells (50, 51). This emphasizes that liver resolution is a complex process involving multiple factors, with debris phagocytosis being just one of the contributing events.

We showed that neutrophils, along with macrophages, rely on complement to phagocytose debris in a model of APAP-induced liver injury (Figures 3E, F). This phenomenon is not limited to the liver, as similar uptake of debris occurred in the lungs of mice with acid-induced lung injury (52). Using confocal microscopy, we observed an average of two DNA-containing phagosomes per cell, consistent with previous findings of macrophages ingesting one or more small cytosolic particles from necrotic cells (53). Interestingly, cells that relied on complement for recruitment did not rely on it for phagocytosis, and *vice versa*, highlighting the existence of multiple pathways for leukocyte recruitment and debris clearance which may compensate each other. Moreover, in a model of FTI of the liver, the phagocytosis of pHRodo-labeled protein-rich necrotic debris was observed, complementing our findings and the one of Wang et al., where neutrophils engulfed nuclear debris (54). Our results showed that in this model phagocytosis in neutrophils and non-classical monocytes is complement-dependent (Figure 4), adding a mechanistic layer to the role of CX_3CR1^+ monocytes in sterile injury resolution. Classical monocytes ($CCR2^{hi}$, CX_3CR1^{lo}) surround the FTI site and transition into non-classical monocytes (CX_3CR1^{hi}, $CCR2^{lo}$) essential for injury repair, a process dependent on IL-10 and IL-4 (55).

Human neutrophils exhibited a pro-resolving phenotype after phagocytosis of necrotic debris, marked by the gene upregulation of IL10, PTGS2, CXCR4, CXCR2 and ANXA1 (Figures 5F-J). This gene expression shifts depend on the type of meal ingested, as illustrated in macrophages, where efferocytosis of apoptotic cells triggers an anti-inflammatory response (56). Research on efferocytosis revealed that the uptake of lipids from apoptotic bodies stimulates sterol receptors (PPARs and Liver X receptors), triggering an anti-inflammatory response via IL-10 and TGF-β production (57, 58). Due to the lipid-rich nature of the debris,

10.3389/fimmu.2024.1512470

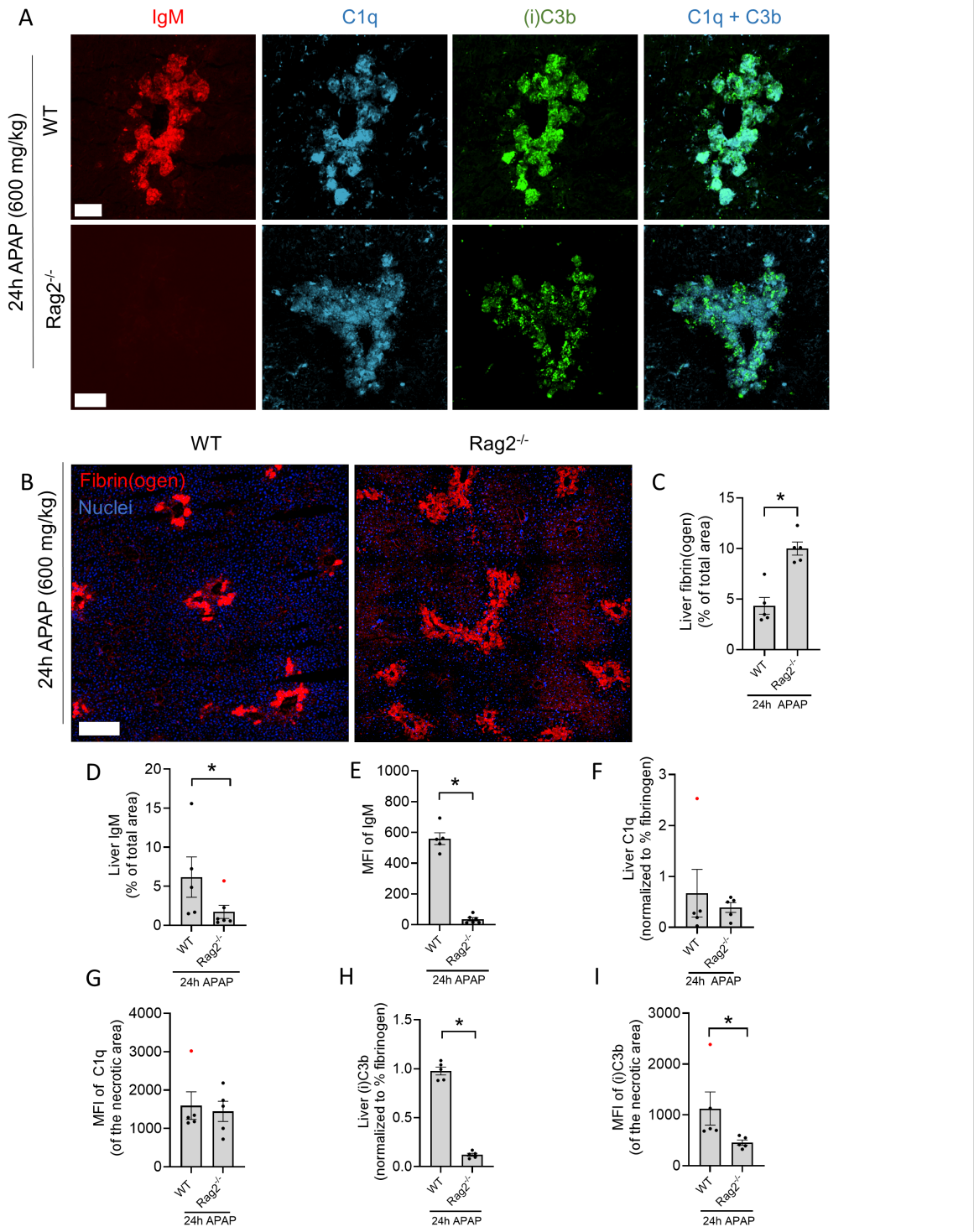

FIGURE 6
The classical complement pathway is activated in response to necrotic debris. **(A)** Representative confocal images of liver cryosections from WT and Rag2$^{-/-}$ mice 24h after an overdose of acetaminophen (APAP; 600 mg/kg). Red: IgM; Cyan: C1q; Green: (i)C3b. Scale bar represents 100 µm. **(B)** Representative confocal images of cryosections from WT and Rag2$^{-/-}$ mice 24h after APAP overdose, stained for fibrin(ogen) and nuclei (Hoechst). Images were acquired with a 25X objective and stitched (3x3). Scale bar represents 200 µm. **(C)** Quantification of area percentage stained with fibrin (ogen) in liver cryosections of WT and Rag2$^{-/-}$ mice 24h after APAP overdose. **(D)** Quantification of area percentage stained with IgM in liver cryosections of WT and Rag2$^{-/-}$ mice 24h after APAP overdose. **(E)** Mean fluorescence intensity (MFI) of IgM staining at the necrotic injury sites in liver cryosections. **(F)** Quantification of C1q deposition in the liver of WT and Rag2$^{-/-}$ mice 24h after APAP overdose, normalized to the degree of fibrin(ogen) staining. **(G)** Mean fluorescence intensity of C1q staining at the necrotic injury sites in liver cryosections. **(H)** Quantification of (i)C3b deposition in the liver of WT and Rag2$^{-/-}$ mice 24h after APAP overdose, normalized to the degree of fibrin(ogen) staining. **(I)** Mean fluorescence intensity of (i)C3b staining at the necrotic injury site of liver cryosections. Image quantifications were pooled from 8 fields of view. Each dot represents a single mouse. At least 5 mice were used per group. Data are represented as mean ± SEM. *p ≤ 0.05 compared to WT mice. Significant outliers are indicated as red dots. APAP, acetaminophen; MFI, Mean fluorescence intensity.

these insights could apply to necrotic cells as well. The upregulated expression of CXCR4 is associated with reverse migration of the neutrophils to the bone marrow, as similarly shown *in vivo* by Wang et al. (54). This process would in theory assist to alleviate the burden of dead cells to be cleared at the injury site when neutrophils undergo apoptosis. The opsonization of debris in the absence of C3 significantly impacted gene expression levels, reducing them to levels comparable to control. This suggests that the specific opsonization process, rather than phagocytosis itself, play a key role in regulating the expression of genes associated with resolution.

The *in vitro* phagocytosis assay showed that both mouse and human neutrophils ingested necrotic debris, however, the phagocytosed volume was reduced in the absence of C1q and C3 (Figure 5). Opsonins affect hydrophobicity and surface charge, consequently influencing receptor interactions (59). This could potentially impact debris removal and explain the larger area of necrotic debris observed in $C3^{-/-}$ mice 48h post-APAP (Figures 2D, E). Also, mechanosensing of the target, which drives actin-based protrusions to mediate particle internalization, might be impaired, possibly due to the reduced stiffness/rigidity of the debris in the absence of C3 (60).

In conclusion, our study demonstrates the crucial role complement proteins play in the opsonization and subsequent phagocytosis of necrotic debris. This mechanism was confirmed in both mouse and human neutrophils, irrespective of the nature of injury (chemical or thermal). This highlights a general complement-dependent pathway for debris clearance specifically for neutrophils. Consequently, individuals with complement deficiencies, whether it is due to genetic factors or auto-immune diseases, might exhibit impaired clearance of necrotic debris, causing prolonged inflammation and poor tissue regeneration. These individuals could potentially benefit from C3 or plasma supplementation to enhance debris clearance and fasten injury recovery.

Data availability statement

The original contributions presented in the study are included in the article/Supplementary Material. Further inquiries can be directed to the corresponding author/s.

Ethics statement

The studies involving humans were approved by ethical committee from University Hospital Leuven (UZ Leuven, S58418). The studies were conducted in accordance with the local legislation and institutional requirements. The participants provided their written informed consent to participate in this study. The animal study was approved by Animal Ethics Committee from KU Leuven (P125/2019). The study was conducted in accordance with the local legislation and institutional requirements.

Author contributions

SV: Investigation, Visualization, Conceptualization, Writing – original draft, Writing – review & editing. MM: Investigation, Validation, Writing – review & editing. EB: Investigation, Writing – review & editing. SS: Investigation, Writing – review & editing. PP: Supervision, Writing – review & editing. PM: Supervision, Conceptualization, Writing – review & editing.

Funding

The author(s) declare financial support was received for the research, authorship, and/or publication of this article. SV and SS hold PhD fellowships from the Research Foundation of Flanders (FWO-Vlaanderen; SB1S56521N and 1116922N, respectively). This work is supported by FWO-Vlaanderen Junior Research Grants (G058421N and G025923N), a KU Leuven C1 grant (14/23/143), a Global PhD Fellowship between KU Leuven and University of Maastricht (GPMU/22/006) and the Rega Foundation.

Conflict of interest

The authors declare that the research was conducted in the absence of any commercial or financial relationships that could be construed as a potential conflict of interest.

The author declared that they were an editorial board member of Frontiers, at the time of submission. This had no impact on the peer review process and the final decision.

Generative AI statement

The author(s) declare that no Generative AI was used in the creation of this manuscript.

Publisher's note

Supplementary material

The Supplementary Material for this article can be found online at: https://www.frontiersin.org/articles/10.3389/fimmu.2024.1512470/full#supplementary-material

References

1. Dunkelberger JR, Song W-C. Complement and its role in innate and adaptive immune responses. *Cell Res*. (2010) 20:34–50. doi: 10.1038/cr.2009.139

2. Fadok VA, De Cathelineau A, Daleke DL, Henson PM, Bratton DL. Loss of phospholipid asymmetry and surface exposure of phosphatidylserine is required for phagocytosis of apoptotic cells by macrophages and fibroblasts. *J Biol Chem*. (2001) 276:1071–7. doi: 10.1074/jbc.M003649200

3. Nauta AJ, Trouw LA, Daha MR, Tijsma O, Nieuwland R, Schwaeble WJ, et al. Direct binding of C1q to apoptotic cells and cell blebs induces complement activation. *Eur J Immunol*. (2002) 32:1726–36. doi: 10.1002/1521-4141(200206)32:6<1726::AID-IMMU1726>3.0.CO;2-R

4. Martin M, Leffler J, Blom AM. Annexin A2 and A5 serve as new ligands for C1q on apoptotic cells. *J Biol Chem*. (2012) 287:33733–44. doi: 10.1074/jbc.M112.341339

5. Wessels MR, Butko P, Ma M, Warren HB, Lage AL, Carroll MC. Studies of group B streptococcal infection in mice deficient in complement component C3 or C4 demonstrate an essential role for complement in both innate and acquired immunity. *Proc Natl Acad Sci U.S.A*. (1995) 92:11490–4. doi: 10.1073/pnas.92.25.11490

6. Smirnov A, Daily KP, Gray MC, Ragland SA, Werner LM, Brittany Johnson M, et al. Phagocytosis via complement receptor 3 enables microbes to evade killing by neutrophils. *J Leukoc Biol*. (2023) 114:1–20. doi: 10.1093/jleuko/qiad028

7. Mueller-Ortiz SL, Drouin SM, Wetsel RA. The alternative activation pathway and complement component C3 are critical for a protective immune response against Pseudomonas aeruginosa in a murine model of pneumonia. *Infect Immun*. (2004) 72:2899–906. doi: 10.1128/IAI.72.5.2899-2906.2004

8. Huang H, Ostroff GR, Lee CK, Agarwal S, Ram S, Rice PA, et al. Relative contributions of dectin-1 and complement to immune responses to particulate β-glucans. *J Immunol*. (2012) 189:312–7. doi: 10.4049/jimmunol.1200603

9. Schuermans S, Kestens C, Marques PE. Systemic mechanisms of necrotic cell debris clearance. *Cell Death Dis*. (2024) 15:557. doi: 10.1038/s41419-024-06947-5

10. Iyer SS, Pulskens WP, Sadler JJ, Butter LM, Teske GJ, Ulland TK, et al. Necrotic cells trigger a sterile inflammatory response through the Nlrp3 inflammasome. *Proc Natl Acad Sci U.S.A*. (2009) 106:20388–93. doi: 10.1073/pnas.0908698106

11. Scaffidi P, Misteli T, Bianchi ME. Release of chromatin protein HMGB1 by necrotic cells triggers inflammation. *Nature*. (2002) 418:191–5. doi: 10.1038/nature00858

12. Ahrens S, Zelenay S, Sancho D, Hanč P, Kjær S, Feest C, et al. F-actin is an evolutionarily conserved damage-associated molecular pattern recognized by DNGR-1, a receptor for dead cells. *Immunity*. (2012) 36:635–45. doi: 10.1016/j.immuni.2012.03.008

13. Zhang Q, Raoof M, Chen Y, Sumi Y, Sursal T, Junger W, et al. Circulating mitochondrial DAMPs cause inflammatory responses to injury. *Nature*. (2010) 464:104–7. doi: 10.1038/nature08780

14. Lind NA, Rael VE, Pestal K, Liu B, Barton GM. Regulation of the nucleic acid-sensing Toll-like receptors. *Nat Rev Immunol*. (2022) 22:224–35. doi: 10.1038/s41577-021-00577-0

15. Imaeda AB, Watanabe A, Sohail MA, Mahmood S, Mohamadnejad M, Sutterwala FS, et al. Acetaminophen-induced hepatotoxicity in mice is dependent on Tlr9 and the Nalp3 inflammasome. *J Clin Invest*. (2009) 119:305–14. doi: 10.1172/JCI35958

16. Marques PE, Oliveira AG, Pereira RV, David BA, Gomides LF, Saraiva AM, et al. Hepatic DNA deposition drives drug-induced liver injury and inflammation in mice. *Hepatology*. (2015) 61:348–60. doi: 10.1002/hep.27216

17. Lai J-J, Cruz FM, Rock KL. Immune sensing of cell death through recognition of histone sequences by C-type lectin-receptor-2d causes inflammation and tissue injury. *Immunity*. (2020) 52:123–135.e6. doi: 10.1016/j.immuni.2019.11.013

18. Schulz O, Hanč P, Böttcher JP, Hoogeboom R, Diebold SS, Tolar P, et al. Myosin II synergizes with F-actin to promote DNGR-1-dependent cross-presentation of dead cell-associated antigens. *Cell Rep*. (2018) 24:419–28. doi: 10.1016/j.celrep.2018.06.038

19. Vandendriessche S, Cambier S, Proost P, Marques PE. Complement receptors and their role in leukocyte recruitment and phagocytosis. *Front Cell Dev Biol*. (2021) 9:624025. doi: 10.3389/fcell.2021.624025

20. Takizawa F, Tsuji S, Nagasawa S. Enhancement of macrophage phagocytosis upon iC3b deposition on apoptotic cells. *FEBS Lett*. (1996) 397:269–72. doi: 10.1016/s0014-5793(96)01197-0

21. Gullstrand B, Mårtensson U, Sturfelt G, Bengtsson AA, Truedsson L. Complement classical pathway components are all important in clearance of apoptotic and secondary necrotic cells. *Clin Exp Immunol*. (2009) 156:303–11. doi: 10.1111/j.1365-2249.2009.03896.x

22. Coss SL, Zhou D, Chua GT, Aziz RA, Hoffman RP, Wu YL, et al. The complement system and human autoimmune diseases. *J Autoimmun*. (2023) 137:102979. doi: 10.1016/j.jaut.2022.102979

23. Mattos MS, Vandendriessche S, Schuermans S, Feyaerts L, Hövelmeyer N, Waisman A, et al. Natural antibodies are required for clearance of necrotic cells and recovery from acute liver injury. *JHEP Rep*. (2024) 6:101013. doi: 10.1016/j.jhepr.2024.101013

24. Marques PE, Antunes MM, David BA, Pereira RV, Teixeira MM, Menezes GB. Imaging liver biology *in vivo* using conventional confocal microscopy. *Nat Protoc*. (2015) 10:258–68. doi: 10.1038/nprot.2015.006

25. Vandesompele J, De Preter K, Pattyn F, Poppe B, Van Roy N, De Paepe A, et al. Accurate normalization of real-time quantitative RT-PCR data by geometric averaging of multiple internal control genes. *Genome Biol*. (2002) 3:RESEARCH0034. doi: 10.1186/gb-2002-3-7-research0034

26. Kopec AK, Joshi N, Cline-Fedewa H, Wojcicki AV, Ray JL, Sullivan BP, et al. Fibrin(ogen) drives repair after acetaminophen-induced liver injury via leukocyte αMβ2 integrin-dependent upregulation of Mmp12. *J Hepatol*. (2017) 66:787–97. doi: 10.1016/j.jhep.2016.12.004

27. Serhan CN, Chiang N. Endogenous pro-resolving and anti-inflammatory lipid mediators: a new pharmacologic genus. *Br J Pharmacol*. (2008) 153 Suppl 1:S200–215. doi: 10.1038/sj.bjp.0707489

28. Schenkein HA, Rutherford B. C3-mediated release of prostaglandin from human monocytes. Behaviour in short-term culture. *Immunology*. (1984) 51:83–91.

29. Powell D, Tauzin S, Hind LE, Deng Q, Beebe DJ, Huttenlocher A. Chemokine signaling and the regulation of bidirectional leukocyte migration in interstitial tissues. *Cell Rep*. (2017) 19:1572–85. doi: 10.1016/j.celrep.2017.04.078

30. Coombs C, Georgantzoglou A, Walker HA, Patt J, Merten N, Poplimont H, et al. Chemokine receptor trafficking coordinates neutrophil clustering and dispersal at wounds in zebrafish. *Nat Commun*. (2019) 10:5166. doi: 10.1038/s41467-019-13107-3

31. Devi S, Wang Y, Chew WK, Lima R, A-González N, Mattar CNZ, et al. Neutrophil mobilization via plerixafor-mediated CXCR4 inhibition arises from lung demargination and blockade of neutrophil homing to the bone marrow. *J Exp Med*. (2013) 210:2321–36. doi: 10.1084/jem.20130056

32. Metzemaekers M, Gouwy M, Proost P. Neutrophil chemoattractant receptors in health and disease: double-edged swords. *Cell Mol Immunol*. (2020) 17:433–50. doi: 10.1038/s41423-020-0412-0

33. Sugimoto MA, Vago JP, Teixeira MM, Sousa LP. Annexin A1 and the resolution of inflammation: modulation of neutrophil recruitment, apoptosis, and clearance. *J Immunol Res*. (2016) 2016:8239258. doi: 10.1155/2016/8239258

34. Manderson AP, Pickering MC, Botto M, Walport MJ, Parish CR. Continual low-level activation of the classical complement pathway. *J Exp Med*. (2001) 194:747–56. doi: 10.1084/jem.194.6.747

35. Singhal R, Ganey PE, Roth RA. Complement activation in acetaminophen-induced liver injury in mice. *J Pharmacol Exp Ther*. (2012) 341:377–85. doi: 10.1124/jpet.111.189837

36. Kim SY, Son M, Lee SE, Park IH, Kwak MS, Han M, et al. High-mobility group box 1-induced complement activation causes sterile inflammation. *Front Immunol*. (2018) 9:705. doi: 10.3389/fimmu.2018.00705

37. Richards JA, Bucsaiova M, Hesketh EE, Ventre C, Henderson NC, Simpson K, et al. Acute liver injury is independent of B cells or immunoglobulin M. *PloS One*. (2015) 10:e0138688. doi: 10.1371/journal.pone.0138688

38. Agrawal A, Shrive AK, Greenhough TJ, Volanakis JE. Topology and structure of the C1q-binding site on C-reactive protein. *J Immunol*. (2001) 166:3998–4004. doi: 10.4049/jimmunol.166.6.3998

39. Nauta AJ, Bottazzi B, Mantovani A, Salvatori G, Kishore U, Schwaeble WJ, et al. Biochemical and functional characterization of the interaction between pentraxin 3 and C1q. *Eur J Immunol*. (2003) 33:465–73. doi: 10.1002/immu.200310022

40. Sørensen IJ, Nielsen EH, Andersen O, Danielsen B, Svehag SE. Binding of complement proteins C1q and C4bp to serum amyloid P component (SAP) in solid contra liquid phase. *Scand J Immunol*. (1996) 44:401–7. doi: 10.1046/j.1365-3083.1996.d01-326.x

41. Quartier P, Potter PK, Ehrenstein MR, Walport MJ, Botto M. Predominant role of IgM-dependent activation of the classical pathway in the clearance of dying cells by murine bone marrow-derived macrophages. *vitro Eur J Immunol*. (2005) 35:252–60. doi: 10.1002/eji.200425497

42. Xu W, Berger SP, Trouw LA, de Boer HC, Schlagwein N, Mutsaers C, et al. Properdin binds to late apoptotic and necrotic cells independently of C3b and regulates alternative pathway complement activation. *J Immunol*. (2008) 180:7613–21. doi: 10.4049/jimmunol.180.11.7613

43. Nauta AJ, Raaschou-Jensen N, Roos A, Daha MR, Madsen HO, Borrias-Essers MC, et al. Mannose-binding lectin engagement with late apoptotic and necrotic cells. *Eur J Immunol*. (2003) 33:2853–63. doi: 10.1002/eji.200323888

44. Markiewski MM, Mastellos D, Tudoran R, DeAngelis RA, Strey CW, Franchini S, et al. C3a and C3b activation products of the third component of complement (C3) are critical for normal liver recovery after toxic injury. *J Immunol*. (2004) 173:747–54. doi: 10.4049/jimmunol.173.2.747

45. He S, Atkinson C, Qiao F, Cianflone K, Chen X, Tomlinson S. A complement-dependent balance between hepatic ischemia/reperfusion injury and liver regeneration in mice. *J Clin Invest*. (2009) 119:2304–16. doi: 10.1172/JCI38289

46. Strey CW, Markiewski M, Mastellos D, Tudoran R, Spruce LA, Greenbaum LE, et al. The proinflammatory mediators C3a and C5a are essential for liver regeneration. *J Exp Med*. (2003) 198:913–23. doi: 10.1084/jem.20030374

47. Khameneh HJ, Ho AWS, Laudisi F, Derks H, Kandasamy M, Sivasankar B, et al. C5a regulates IL-1β Production and leukocyte recruitment in a murine model of monosodium urate crystal-induced peritonitis. *Front Pharmacol*. (2017) 8:10. doi: 10.3389/fphar.2017.00010

48. Holt MP, Cheng L, Ju C. Identification and characterization of infiltrating macrophages in acetaminophen-induced liver injury. *J Leukoc Biol*. (2008) 84:1410–21. doi: 10.1189/jlb.0308173

49. Karlmark KR, Weiskirchen R, Zimmermann HW, Gassler N, Ginhoux F, Weber C, et al. Hepatic recruitment of the inflammatory Gr1+ monocyte subset upon liver injury promotes hepatic fibrosis. *Hepatology*. (2009) 50:261–74. doi: 10.1002/hep.22950

50. Venkatesha RT, Berla Thangam E, Zaidi AK, Ali H. Distinct regulation of C3a-induced MCP-1/CCL2 and RANTES/CCL5 production in human mast cells by extracellular signal regulated kinase and PI3 kinase. *Mol Immunol*. (2005) 42:581–7. doi: 10.1016/j.molimm.2004.09.009

51. Purwar R, Wittmann M, Zwirner J, Oppermann M, Kracht M, Dittrich-Breiholz O, et al. Induction of C3 and CCL2 by C3a in keratinocytes: a novel autocrine amplification loop of inflammatory skin reactions. *J Immunol*. (2006) 177:4444–50. doi: 10.4049/jimmunol.177.7.4444

52. Oved JH, Paris AJ, Gollomp K, Dai N, Rubey K, Wang P, et al. Neutrophils promote clearance of nuclear debris following acid-induced lung injury. *Blood*. (2021) 137:392–7. doi: 10.1182/blood.2020005505

53. Brouckaert G, Kalai M, Krysko DV, Saelens X, Vercammen D, Ndlovu MN, et al. Phagocytosis of necrotic cells by macrophages is phosphatidylserine dependent and does not induce inflammatory cytokine production. *Mol Biol Cell*. (2004) 15:1089–100. doi: 10.1091/mbc.e03-09-0668

54. Wang J, Hossain M, Thanabalasuriar A, Gunzer M, Meininger C, Kubes P. Visualizing the function and fate of neutrophils in sterile injury and repair. *Science*. (2017) 358:111–6. doi: 10.1126/science.aam9690

55. Dal-Secco D, Wang J, Zeng Z, Kolaczkowska E, Wong CHY, Petri B, et al. A dynamic spectrum of monocytes arising from the in *situ* reprogramming of CCR2+ monocytes at a site of sterile injury. *J Exp Med*. (2015) 212:447–56. doi: 10.1084/jem.20141539

56. Chung EY, Liu J, Homma Y, Zhang Y, Brendolan A, Saggese M, et al. Interleukin-10 expression in macrophages during phagocytosis of apoptotic cells is mediated by homeodomain proteins Pbx1 and Prep-1. *Immunity*. (2007) 27:952–64. doi: 10.1016/j.immuni.2007.11.014

57. A-Gonzalez N, Bensinger SJ, Hong C, Beceiro S, Bradley MN, Zelcer N, et al. Apoptotic cells promote their own clearance and immune tolerance through activation of the nuclear receptor LXR. *Immunity*. (2009) 31:245–58. doi: 10.1016/j.immuni.2009.06.018

58. Mukundan L, Odegaard JI, Morel CR, Heredia JE, Mwangi JW, Ricardo-Gonzalez RR, et al. PPAR-delta senses and orchestrates clearance of apoptotic cells to promote tolerance. *Nat Med*. (2009) 15:1266–72. doi: 10.1038/nm.2048

59. Panico S, Capolla S, Bozzer S, Toffoli G, Dal Bo M, Macor P. Biological features of nanoparticles: protein corona formation and interaction with the immune system. *Pharmaceutics*. (2022) 14:2605. doi: 10.3390/pharmaceutics14122605

60. Jaumouillé V, Cartagena-Rivera AX, Waterman CM. Coupling of β2 integrins to actin by a mechanosensitive molecular clutch drives complement receptor-mediated phagocytosis. *Nat Cell Biol*. (2019) 21:1357–69. doi: 10.1038/s41556-019-0414-2